SWTV-ACE: Spatially Weighted Regularization Based Attenuation Coefficient Estimation Method for Hepatic Steatosis Detection

Farah Deeba[1]([✉]) [iD], Caitlin Schneider[1], Shahed Mohammed[1] [iD],
Mohammad Honarvar[1], Edward Tam[2], Septimiu Salcudean[1],
and Robert Rohling[1,3]

[1] Department of Electrical and Computer Engineering,
The University of British Columbia, Vancouver, BC, Canada
`farahdeeba@ece.ubc.ca`
[2] The Lair Centre, Vancouver, BC, Canada
[3] Department of Mechanical Engineering, The University of British Columbia,
Vancouver, BC, Canada

Abstract. We present a spatially weighted total variation regularization based method for measuring the ultrasonic attenuation coefficient estimate (ACE). We propose a new approach to adapt the local regularization by employing envelope signal-to-noise-ratio deviation, an indicator of tissue inhomogeneity. We evaluate our approach with simulations and demonstrate its utility for hepatic steatosis detection. The proposed method significantly outperforms the reference phantom method in terms of accuracy (9% reduction in ACE error) and precision (52% reduction in ACE standard deviation) for the homogeneous phantom. The method also exceeds the performance of uniform TV regularization in inhomogeneous tissue with high backscatter variation. The ACE computed using the proposed method showed a strong correlation of 0.953 (p = 0.003) with the MRI proton density fat fraction, whereas the reference phantom method and uniform TV regularization yield correlations of 0.71 (p = 0.11) and 0.44 (p = 0.38), respectively. The equivalence of SWTV-ACE with MRI proton density fat fraction, which is the current gold standard for hepatic steatosis detection, shows the potential of the proposed method to be a point-of-care tool for hepatic steatosis detection.

Keywords: Attenuation coefficient estimate · Nonalcoholic fatty liver disease · Steatosis · Proton density fat fraction · Envelope signal-to-noise ratio deviation

1 Introduction

Accompanying the pandemic spread of obesity, nonalcoholic fatty liver disease (NAFLD) is emerging as the most common cause of chronic liver disease with an

estimated global prevalence of 25% [5]. From the early stage defined as simple hepatic steatosis (excessive fat accumulation in liver cells), NAFLD can potentially progress into advanced fibrosis, cirrhosis and malignancy. Liver biopsy is not feasible for routine screening due to its potential risk and prohibitive cost. Thus, there is a significant interest in developing reliable, inexpensive and non-invasive biomarkers to detect and monitor the progression of NAFLD.

Fat droplets in the fatty liver cause cellular ballooning, which affects the ultrasonic scattering process, resulting in an increase in attenuation coefficient estimate (ACE). Based on this principle, ACE can be utilized as a promising tool to detect and quantify hepatic steatosis [9]. Unfortunately, ACE methods based on a sliding window approach suffer from the trade-off between image resolution and estimation precision and accuracy. Larger windows improve accuracy and precision by reducing the spatial variation noise inherent in ultrasonic scattering, whereas smaller windows better resolve the underlying structure [7]. More recently, researchers have shown that regularization incorporating a spatial prior can improve ACE results in terms of precision and resolution in homogeneous regions [1,11]. However, variation in scatterer size and concentration inevitably creates inhomogeneity in tissue, which results in a large error in ACE estimation [8]. This issue, while unaddressed in [1], was tackled using different regularization weights for inhomogeneous phantoms (variable backscatter with uniform ACE) than that used for homogeneous phantoms (variable ACE with uniform backscatter) in [11]. Clearly, different regularization weights for different phantoms would not be applicable for biological tissue, where variation in ACE and backscatter may occur simultaneously. Moreover, using uniform regularization across the image as in [1,11], would lead to over-smoothing in homogeneous regions in an attempt to compensate for the local inhomogeneities.

In this work, we propose, for the first time, a spatially weighted total variation regularization based reference phantom method for ACE estimation. The contributions of the paper are: (1) modulating the amount of regularization depending on the inhomogeneity information, (2) derivation of the spatially weighted regularization parameters from the tissue inhomogeneity indicator: envelope signal-to-noise ratio deviation [2], and (3) introducing the novel use of spatially weighted regularization within the ACE computation framework. We validate the proposed method on simulation and phantom data. Finally, we demonstrate the successful application of the proposed method in computing ACE for liver *in vivo* and in assessing the extent of hepatic steatosis with Magnetic Resonance Imaging Proton Density Fat Fraction (MRI-PDFF) imaging as a reference.

2 Method

2.1 Spatially Weighted Regularization Based ACE (SWTV-ACE)

The ultrasound ACE is a measure of ultrasound amplitude dissipation due to the combined effect of scattering and absorption, whereas the dissipation associated with the scattering is small compared to absorption (less than 10% for typical

biological tissue) [3]. The standard way is to compute ACE using the reference phantom method [12]. According to this method, the radiofrequency (RF) data are acquired from both the tissue sample and a reference phantom using the same transducer and system settings.

ACE is computed in a $m \times n$ grid using a frequency band discretized at r points. For a RF signal window centered at $(i, j)[i \in (1, m), j \in (1, n)]$ location, the ratio of the power spectrum S from the sample to the reference phantom at frequency $f_k, k \in (1, r)$ can be written as [2,11]:

$$RS_{i,j,k} = \frac{S_{i,j,k}^s}{S_{i,j,k}^r} = \frac{A_{i,j,k}^s B_{i,j,k}^s}{A_{i,j,k}^r B_{i,j,k}^r} = \frac{e^{-4\alpha_{i,j}^s f_k z_{i,j}}}{e^{-4\alpha_{i,j}^r f_k z_{i,j}}} \cdot \frac{B_{i,j}^s}{B_{i,j}^r}. \tag{1}$$

Here, the s and r superscript denote sample and reference, respectively. A is the total attenuation effect from the transducer surface to the center of the respective RF signal window, B is the backscatter coefficient (BSC), z is the axial distance from the transducer surface to the center of the corresponding time-gated RF signal window, and α is the effective ACE for the total ultrasound propagation path z. After taking the natural logarithm, Eq. 1 reduces to:

$$\ln[RS_{i,j,k}] = -4(\alpha_{i,j}^s - \alpha_{i,j}^r)f_k z_{i,j} + \ln\frac{B_{i,j}^s}{B_{i,j}^r}. \tag{2}$$

Substituting the following variables in Eq. 2 as: $\ln[RS_{i,j,k}] = Y_{i,j,k}, \alpha_{i,j}^r - \alpha_{i,j}^s = \alpha_{i,j}, \ln\frac{B_{i,j}^s}{B_{i,j}^r} = \beta_{i,j}$, we get,

$$Y_{i,j,k} = -4\alpha_{i,j}f_k z_{i,j} + \beta_{i,j}. \tag{3}$$

The above equation can be written in a matrix form: $y = Ax + \eta$, where η denotes Gaussian noise with zero mean and standard deviation σ, where

$$A = \begin{bmatrix} 4z_{1,1}f_1 \dots & 0 & 1 \dots 0 \\ \vdots & \ddots & \vdots & \vdots \ddots \vdots \\ 0 & \dots 4z_{m,n}f_1 & 0 \dots 1 \\ \vdots & \vdots & \vdots & \vdots \vdots \vdots \\ 4z_{1,1}f_r \dots & 0 & 1 \dots 0 \\ \vdots & \ddots & \vdots & \vdots \ddots \vdots \\ 0 & \dots 4z_{m,n}f_r & 0 \dots 1 \end{bmatrix}, y = \begin{bmatrix} Y_{1,1,1} \\ \vdots \\ Y_{m,n,1} \\ \vdots \\ Y_{1,1,r} \\ \vdots \\ Y_{m,n,r} \end{bmatrix}, x = \begin{bmatrix} \alpha_{1,1} \\ \vdots \\ \alpha_{m,n} \\ \beta_{1,1} \\ \vdots \\ \beta_{m,n} \end{bmatrix}.$$

We propose to solve the following spatially weighted optimization problem for the reconstruction of $x = [\alpha, \beta]$ from the noisy estimation Y:

$$\hat{x} = \arg\min_x \{\|y - Ax\|_2^2 + \lambda_1 TV(\alpha) + \lambda_2 SWTV(\beta)\}, \tag{4}$$
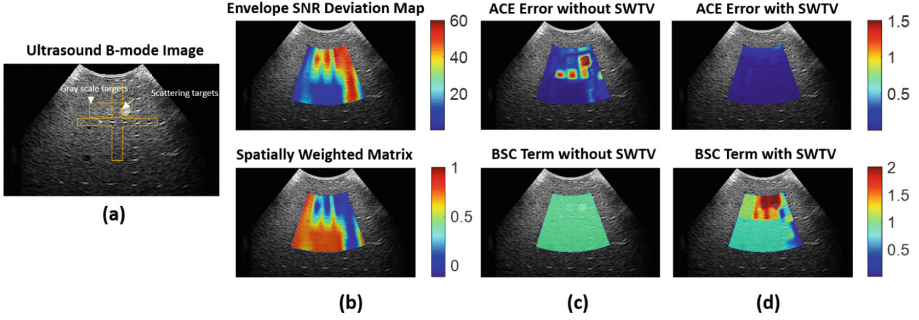
Fig. 1. Feasibility test of the proposed SWTV-ACE method on a tissue-mimicking phantom. (a) Ultrasound image of the phantom with backscatter variation; (b) Spatially weighted matrix formation as a function of the envelope SNR deviation map; (c) & (d) ACE and BSC results with and without SWTV.

where the first term is the data fidelity term, the second and third terms are the anisotropic TV based regularization term, and λ_1 and λ_2 are the regularization weights. The TV operator is defined as: $TV(\alpha) = \sum_{i,j} |\alpha_{i+1,j} - \alpha_{i,j}| + |\alpha_{i,j+1} - \alpha_{i,j}|$, and

$$SWTV(\beta) = \sum_{i,j} W_\beta^{i,j}(|\beta_{i+1,j} - \beta_{i,j}| + |\beta_{i,j+1} - \beta_{i,j}|).$$

Here we have employed a spatially weighted total variation regularization on the BSC term, β. The reason is that a change in scattering affects the power spectrum of the ultrasound RF data, which should be accounted into the BSC term, β. However, the assumption of constant backscatter in the reference phantom method and uniform piece-wise homogeneity in uniform TV regularization fail to account for the change in scattering into the BSC term and consequently result in inaccurate computation of ACE. For the regions associated with changes in backscatter, β should be lightly regularized to decrease the penalty on their variation. Therefore, we propose incorporating a spatially weighted matrix W_β into the regularization of β to account for the backscatter variation.

2.2   Derivation of Spatially Weighted Matrix

According to a previous study, envelope SNR deviation is a useful criterion to indicate inhomogeneity, i.e., variation in backscatter. Envelope SNR Deviation, ΔSNR_e is defined as:

$$\Delta SNR_e = \frac{|SNR_e - SNR_{opt}|}{SNR_{opt}} \times 100\%, \tag{5}$$

where SNR_e is defined as the ratio of the mean to the standard deviation of the RF signal envelope. $SNR_{opt} = 1.91$, which is the average envelope SNR of

a Rayleigh distribution, the characteristic distribution of a RF signal spectrum, arising from a large number of randomly distributed scatterers of identical sizes.
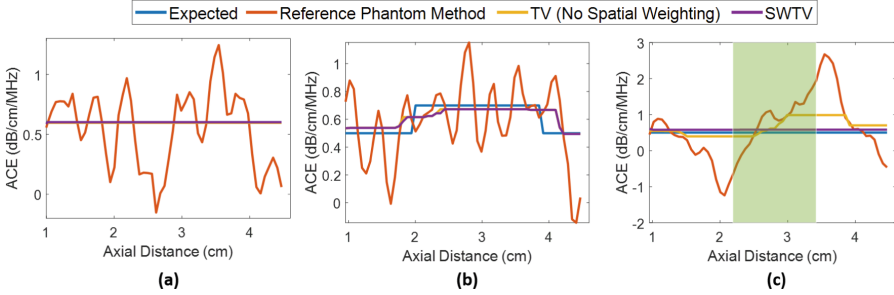

Fig. 2. ACE results for simulated phantoms: (a) phantom 1 (uniform ACE and BSC); (b) phantom 2 (variable ACE and uniform BSC); and (c) phantom 3 (uniform ACE and variable BSC).

To validate the applicability of ΔSNR_e as an indicator of inhomogeneity, we performed a feasibility analysis of RF data acquired from an ultrasound phantom (Model 040GSE) manufactured by CIRS (Norfolk, VA, USA). The phantom contains two different types of targets: scattering targets and gray scale targets (Fig. 1a). The scattering targets are made of nylon monofilaments and contain scatterers of different size, whereas the gray scale targets contain scatterers with a different density. As we plot the ΔSNR_e map, the targets can be distinguished with high ΔSNR_e values (Fig. 1b). Ideally, the phantom has a uniform ACE value of 0.7 dB/cm/MHZ, and variable BSC values at the locations of the targets (BSC values were not reported by the manufacturer). Interestingly, computing the ACE and BSC using both the reference phantom and the uniform TV regularization yield high ACE errors at the target locations while both the methods fail to identify the variation in the BSC term (Fig. 1c). As a solution to this problem, we propose to form a spatially weighted matrix, W_β as a function of ΔSNR_e, to adaptively regularize the BSC parameter:

$$W_\beta(\Delta SNR_e) = \frac{a}{1 + \exp[b.(\Delta SNR_e - \Delta SNR_e^{\min})]}, \tag{6}$$

where a and b are constants. $\Delta SNR_e^{\min}$ is a nominal ΔSNR_e value for which the associated regions can be considered to be homogeneous. As ΔSNR_e remains much smaller than $\Delta SNR_e^{\min}$, the weighting has little effect on the regularization. On the other hand, the weight will decrease as ΔSNR_e increases resulting in relaxation of the regularization effect on the BSC term. By applying the proposed spatially weighted TV regularization, the ACE error was significantly reduced, where the BSC term captures the backscatter variation at the target locations (Fig. 1d).
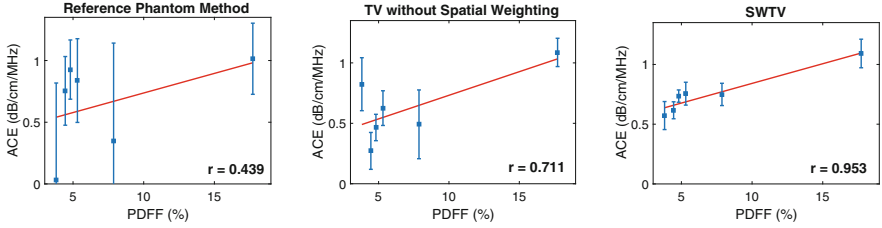
Fig. 3. *In vivo* human liver ACE from six patients and their correlation with proton density fat fraction. The error bars show the standard deviation whereas the square represents the mean calculated over a region-of-interest.

3 Experiments and Results

The proposed method was implemented in MATLAB 2018a (The MathWorks Inc., Natick, MA, USA). The optimization problem was solved using the convex optimization toolbox CVX in MATLAB [4]. We evaluated the proposed SWTV-ACE method on several datasets including simulations and liver *in vivo*. We compared the performance of the proposed method against the reference phantom method [12] and uniform TV regularization. The dimensions of the sliding windows were selected to be 15 scanlines (10 wavelengths) laterally and 8.5 mm (10 wavelengths) axially with an 80% overlap in both directions for all the methods. We set $\lambda_1 = 2^1$, $\lambda_2 = 2^{-1}$ for the regularization weights and $a = 5, b = 0.09$, and $\Delta SNR_e^{\min} = 15$ as the parameters of the spatially weighted matrix, W_β (Fig. 3; Eqs. 4 and 6).

3.1 Simulations

We used the k-Wave toolbox to simulate three numerical phantoms [10]. Phantom 1 consisted of homogeneous medium with uniform ACE (0.6 dB/cm/MHz) and uniform BSC. Phantom 2 had uniform BSC and variable ACE, where the background ACE was 0.5 dB/cm/MHz, and the inclusion ACE was 0.7 dB/cm/MHz. Phantom 3 had variable BSC and uniform ACE (0.5 dB/cm/MHz), where the inside inclusion had a higher BSC compared to the background. Also, we simulate a phantom with uniform ACE (0.6 dB/cm/MHz) and uniform BSC, which would be used as the reference phantom to compensate for the system dependence.

For phantom 1 and phantom 2, the SWTV-ACE method gives similar performance as that obtained from the uniform TV regularization as these phantoms have uniform BSC. In both methods, ACE error is reduced significantly (<1%) compared to the reference phantom method (10%), whereas the ACE variance is reduced to ∼1% from 53% obtained using the reference phantom method (Fig. 2(a)). For phantom 2, both uniform TV and SWTV-ACE method can identify the ACE transition in the center inclusion (standard deviation ∼11%) opposed to the reference phantom method where the transition remains occluded

with high variance of ACE (63%) (Fig. 2(b)). Finally, the SWTV-ACE method shows superior performance for phantom 3 where both the reference phantom and the uniform TV regularization exhibit underestimation and overestimation of ACE centering the high backscatter inclusion (shaded area in Fig. 2(c)) [8]. On the contrary, the spatial weighting enables the proposed method to reconstruct the expected uniform ACE map with 16% error and standard deviation <1%.
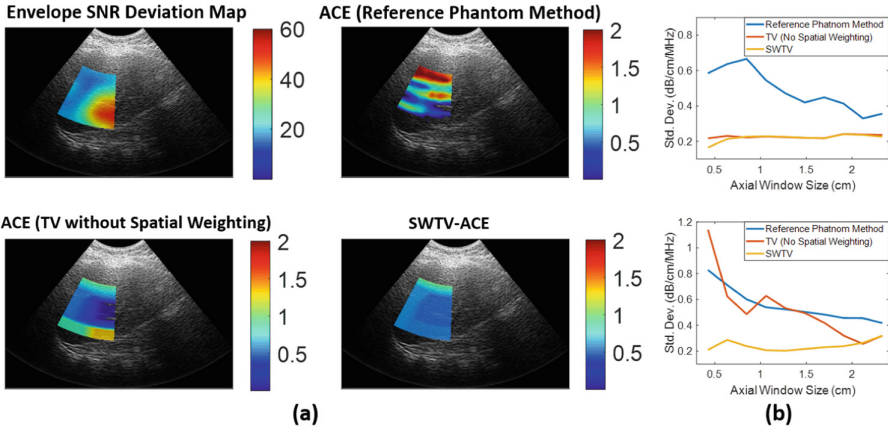
Fig. 4. (a) An example of ACE computation for *in vivo* human liver using three different methods. (b) Effect of window size on estimation variance of ACE for a homogeneous region-of-interest (top) and inhomogeneous region-of-interest (bottom).

3.2   *In Vivo* Liver: Steatosis Detection

We validated the efficacy of the proposed method to detect hepatic steatosis based on six patients, who underwent MRI in a 3.0 T system (Philips Achieva, Philips Medical Systems). MRI proton density fat fraction (MRI-PDFF) computed from the MRI data was used as a gold standard for hepatic steatosis quantification, which strongly correlates with histological steatosis grading [6]. The patients also underwent ultrasound examination with an Ultrasonix SonixTouch machine (Analogic, Canada), the RF data from which were used to compute ACE. The correlation between MRI-PDFF and ACE values was calculated to evaluate the performance of the SWTV-ACE method to detect hepatic steatosis.

The correlation between ACE computed using the reference phantom method to MRI-PDFF was 0.44 (p = 0.3838). The TV method yields a better correlation performance (r = 0.71, p = 0.1132). The SWTV-ACE method outperforms both of these methods with a correlation of 0.953 (p =.003). Therefore, SWTV-ACE method demonstrated an improved correlation with MRI-PDFF even with small window size, therefore extending the trade-off between window size and precision inherent in conventional ACE computation.

We also showed an example of ACE computation for *in vivo* liver, where an inhomogeneity indicated by high envelope SNR deviation causes significant variation of ACE (including negative ACE values) computed using the reference phantom method and the uniform TV regularization method (Fig. 4(a)). However, SWTV-ACE method yields positive ACE values with low estimation variance. Additionally, we investigated the effect of axial window size on the the estimation variation of ACE for a homogeneous region-of-interest ($\max(\Delta SNR_e) < 20\%$) and an inhomogeneous region-of-interest in liver ($mean(\Delta SNR_e) > 20\%$). For the homogeneous case, both uniform TV regularization and SWTV-ACE methods maintain similar standard deviation for different window sizes, whereas the reference phantom method exhibits the trade-off where estimation precision improves with increasing window size. For the inhomogeneous case, however, SWTV-ACE method outperforms both the reference phantom method and the uniform TV regularization by maintaining similar standard deviation for different window sizes (Fig. 4(b)). Therefore, SWTV-ACE effectively improves the quality of ACE computation by reducing the variability in the estimates irrespective of window size. The improved resolution will be beneficial to provide information about the local variation within the liver, whereas the improved precision would be required to qualify as a reliable diagnostic tool.

4   Conclusion

We propose a new spatially weighted regularization based ACE estimation method. The goal was to modulate the regularization in the inhomogeneous regions using a weight function formulated as a function of envelope signal-to-noise ratio, an indicator of tissue heterogeneity. The proposed method was able to attain improved precision without compromising the resolution of ACE for both homogeneous and inhomogeneous regions with high backscatter variation. The strong correlation of the ACE measurements with the current gold-standard MRI-PDFF demonstrated the potential application of the proposed method for the detection of liver steatosis.

References

1. Coila, A.L., Lavarello, R.: Regularized spectral log difference technique for ultrasonic attenuation imaging. IEEE Trans. Ultrason. Ferroelectr. Freq. Control **65**(3), 378–389 (2017). https://doi.org/10.1109/TUFFC.2017.2719962
2. Deeba, F., et al.: Attenuation coefficient estimation of normal placentas. Ultras. Med. Biol. **45**(5), 1081–1093 (2019). https://doi.org/10.1016/j.ultrasmedbio.2018.10.015

3. Flax, S.W., Pelc, N.J., Glover, G.H., Gutmann, F.D., McLachlan, M.: Spectral characterization and attenuation measurements in ultrasound. Ultrason. Imaging **5**(2), 95–116 (1983). https://doi.org/10.1016/0161-7346(83)90013-5

4. Grant, M., Boyd, S., Ye, Y.: CVX: Matlab software for disciplined convex programming (2008)

5. Loomba, R., Sanyal, A.J.: The global NAFLD epidemic. Nat. Rev. Gastroenterol. Hepatol. **10**(11), 686 (2013). https://doi.org/10.1038/nrgastro.2013.171

6. Noureddin, M., et al.: Utility of magnetic resonance imaging versus histology for quantifying changes in liver fat in nonalcoholic fatty liver disease trials. Hepatology **58**(6), 1930–1940 (2013). https://doi.org/10.1002/hep.26455

7. Oelze, M.L., O'Brien Jr., W.D.: Defining optimal axial and lateral resolution for estimating scatterer properties from volumes using ultrasound backscatter. J. Acoust. Soc. Am. **115**(6), 3226–3234 (2004). https://doi.org/10.1121/1.1739484

8. Pawlicki, A.D., O'Brien Jr., W.D.: Method for estimating total attenuation from a spatial map of attenuation slope for quantitative ultrasound imaging. Ultrason. Imaging **35**(2), 162–172 (2013). https://doi.org/10.1177/0161734613478695

9. Pohlhammer, J.D., O'Brien Jr, W.D.: The relationship between ultrasonic attenuation and speed in tissues and the constituents: water, collagen, protein and fat. In: Medical physics of CT and Ultrasound: Tissue Imaging and Characterization. American Institute of Physics (1980)

10. Treeby, B.E., Jaros, J., Rendell, A.P., Cox, B.: Modeling nonlinear ultrasound propagation in heterogeneous media with power law absorption using a k-space pseudospectral method. J. Acoust. Soc. Am. **131**(6), 4324–4336 (2012). https://doi.org/10.1121/1.4712021

11. Vajihi, Z., Rosado-Mendez, I.M., Hall, T.J., Rivaz, H.: Low variance estimation of backscatter quantitative ultrasound parameters using dynamic programming. IEEE Trans. Ultrason. Ferroelectr. Freq. Control **65**(11), 2042–2053 (2018). https://doi.org/10.1109/TUFFC.2018.2869810

12. Yao, L.X., Zagzebski, J.A., Madsen, E.L.: Backscatter coefficient measurements using a reference phantom to extract depth-dependent instrumentation factors. Ultrason. Imaging **12**(1), 58–70 (1990). https://doi.org/10.1177/016173469001200105